Celal Bayar University Journal of Science

The Thermal Performance of The Plate-fin Heat Sink under Natural Convection at Different Power Levels and Ambient Temperatures

Mesut Abuşka[1*], Vahit Çorumlu[2]

[1]Manisa Celal Bayar University, Akhisar Vocational School, Dept. of Machine 45200, Manisa, Türkiye
[2]Manisa Celal Bayar University, Akhisar Vocational School, Dept. of Electrical and Energy 45200, Manisa, Türkiye

* mesut.abuska@cbu.edu.tr
* Orcid No: 0000-0003-2686-9786

Received: 13 August 2024
Accepted: 24 September 2024
DOI: 10.18466/cbayarfbe.1532575

Abstract

The thermal performance of a flat heat sink and a plate-fin heat sink was experimentally compared under natural convection conditions at thermal powers of 16.5 W and 33 W and ambient temperatures of 30°C and 40°C. For the same heating powers, surface and junction temperatures increased as the ambient temperature rose from 30°C to 40°C, but the increase was not as much as the ambient temperature change. For the flat heat sink, the increase in junction temperature was 5°C at 16.5 W and 6.68°C at 33 W. For the plate-fin heat sink, the increase in junction temperature was 3.55°C at 16.5 W and 4.47°C at 33 W. The increase in surface temperature for the flat heat sink was 5.35°C at 16.5 W and 5.91°C at 33 W, while for the plate-fin heat sink, the surface temperature increase was 4.76°C at 16.5 W and 2.22°C at 33 W. The thermal resistance of the flat heat sink was around 4 K/W, while for the plate-fin heat sink, it ranged between 2-2.5 K/W, providing approximately twice the advantage in thermal resistance for the plate-fin model compared to the flat model. Under all conditions, the Rayleigh number (Ra) significantly decreased with the increase in ambient temperature but increased with the applied thermal power. Thus, the increase in Rayleigh number with power was more pronounced in the plate-fin model, indicating a more significant effect. In the plate-fin model, the fin efficiency slightly decreased with the increase in ambient temperature, from 0.63 to 0.62 at 16.5 W and from 0.65 to 0.64 at 33 W.

Keywords: heat sink, plate-fin, natural convection, ambient temperature, power.

1. Introduction

Heat sinks are passive heat exchangers that transfer heat generated by electronic or mechanical devices to a fluid, thus maintaining the device temperature within the desired range. Heat sinks are commonly used in the thermal management of CPUs, GPUs, RAM modules, laser systems, power transistors such as light emitting diodes (LEDs), SSRs (Solid State Relays), and other high-power semiconductor devices such as optoelectronics. As the electrical and electronics industry rapidly evolves, the devices in use are experiencing increased electrical and thermal loads while their sizes are being reduced or there is a demand for miniaturization. The goal of size reduction is to decrease the overall volume and reduce the raw material inputs required for manufacturing. One of the most critical factors affecting the lifespan of electronic components is the operation of these components above the specified safe temperature ranges. The most common and effective method to ensure that devices operate within the appropriate temperature range is the use of heat sinks, which are both efficient and relatively economical. Approximately 55% of electronic equipment failures are attributed to systems operating at undesirably high temperatures [1]. Operating at elevated temperatures significantly shortens the lifespan of these devices, making thermal management in electronic systems increasingly crucial alongside technological advancements. Heat sinks are typically employed with natural convection in applications without space or volume constraints and with forced convection in constrained electronic applications. Key factors influencing the cooling performance of heat sinks include the material used in manufacturing, surface geometry, fin design, and the type of convection. In this context, the literature has focused on fin geometry, arrangement, size,

structure, and modifications to enhance cooling performance by increasing the heat transfer area and creating turbulence regions while maintaining acceptable pressure drop and flow blockage levels. Parameters such as flow rate and ambient temperature also play a significant role in performance. Design principles prioritize simplicity, reliability, and minimizing manufacturing and operational costs. Although extensive research on heat sinks is in the literature, this study reviews the most relevant works based on the specific geometry, convection type, and experimental test characteristics under investigation.

Doğan and Doğan [2] experimentally investigated the thermal performance of a plate-fin heat sink (PF_{hs}) under natural convection conditions with fin heights ranging from 15 to 40 mm, a base fin spacing of 12 mm, a fin thickness of 3 mm, and varying gap ratios between the fin tips and the base from 0.25 to 1. They found that the optimal gap ratio for fins providing the best thermal performance was between C=0.50 and C=0.75, with this optimal ratio being primarily dependent on fin height and the Rayleigh number. In the study by Haghighi et al. [3], the thermal performance of heat sinks with plate-type and cubic plate-type fins under natural convection was evaluated at Rayleigh numbers of 8-9.5x106, heating powers of 10-120 W, fin spacing of 5-12 mm, and fin counts of 5-9. A 10-41.6% increase in heat transfer was recorded in the cubic plate-type fin heat sink. As the fin spacing increased, thermal resistance decreased, but the increase in fin number did not positively contribute to heat transfer. The optimal configuration for the cubic plate-type heat sink was seven fins with an 8.5 mm fin spacing. Shen et al. [4] examined the effect of eight different orientations on the thermal performance of a PF_{hs} under natural convection. They concluded that the mismatch between the heat transfer area and flow blockage was a key factor affecting heat transfer under both natural and forced convection and that fin density played a significant role in orientation. Şevik and Özdilli [5] studied the effect of different fin geometries, such as trapezoidal and grooved, on the thermal performance of plate-type heat sinks. These geometries were designed with fin heights of 10-20 mm and analyzed numerically using SolidWorks Flow Simulation at thermal powers of 5W and 10W. The heat sinks were compared regarding temperature distribution, material weight, fin height, and surface area. The trapezoidal geometry performed best, followed closely by the trapezoidal-grooved geometry. At 5W, the maximum temperature difference between models was 3°C for a 20 mm fin height and 6°C for a 10 mm fin height. At 10W, the maximum temperature difference was 4°C for the 20 mm fins and 8°C for the 10 mm fins. The modeling results indicated that maximum temperature was more affected by fin height than fin geometry. Özdilli and Şevik [6] designed three types of heat sinks aimed at minimizing junction temperature: a trapezoidal plate-type finned model (Model-1), a chamfered trapezoidal finned model (Model-2), and a standard plate-type heat sink for comparison. Under natural convection, Models 1 and 2 achieved thermal resistance values that were 14-17% better than the standard model. Models 1 and 2 also provided a 5-15% advantage in junction temperature compared to the standard model. Yalçın [7] used Finite Element Modeling (FEM) to study the effects of fin geometry (straight and wavy), fin count (4-6-8), fin thickness, and material type (aluminum and copper) on the thermal performance of plate-type heat sinks exposed to temperatures of 50, 150, and 250°C. The study found that increasing the fin number while decreasing the fin thickness resulted in higher temperature differences in the heat sinks, thereby increasing the heat transfer rates. Feng et al. [8] examined the performance of standard and cross PF_{hs}s under natural convection, finding an 11% increase in total heat transfer coefficient for the cross model without changing material or cost. Banerjee et al. [9] conducted a numerical analysis of plate-type, cylindrical, and conical finned heat sinks with identical surface areas, identifying the conical model as the most efficient fin structure despite the lowest efficiency being observed in the cylindrical type. They determined the PF_{hs} as the most effective fin structure. Altun and Ziylan [10] experimentally studied heat transfer in vertical sinusoidal wavy fins under natural convection. Their results showed that wavy fins provided better heat transfer than plate fins; however, beyond a certain wave width, the increased blockage of fluid flow negatively impacted natural convection. They also noted that a significant portion of total heat transfer occurred through radiation and that this should be considered in the design of finned heat sinks for natural convection applications. Charles and Wang [11] compared the performance of plate, trapezoidal, and inverted trapezoidal fin heat sinks under natural convection at heating powers ranging from 3 to 20 W. While the heat transfer coefficient of the standard plate-fin model was higher than that of the trapezoidal model, the inverted trapezoidal model provided a 25% and 10% advantage over the trapezoidal and standard plate models, respectively. The advantage of the inverted trapezoidal model was attributed to a larger temperature difference and improved air passage. Do et al. [12] investigated the thermal resistance of plate-type heat sinks for cooling concentrated photovoltaic modules under natural convection, considering input power and tilt angle. They found that the optimal fin spacing depended on temperature difference and tilt angle.

In the literature, studies on forced convection are predominant, studies on natural convection are rare, and the effect of ambient temperature on performance is almost negligible. This study aims to experimentally determine the performance of PF_{hs} at different powers and ambient temperatures in natural convection. In addition, the performance comparison was made with a flat heat sink [13].

Celal Bayar University Journal of Science
Volume 20, Issue 3, 2024, p 91-99
Doi: 10.18466/cbayarfbe.1532575

2. Experimental Setup and Thermal Analysis

2.1. Experimental setup

In this study, a PF_{hs} was experimentally tested under natural convection conditions at different heating powers and ambient temperatures, and a flat heat sink (F_{hs}) was also used for comparison. In order to address the effect of ambient temperature and power difference on thermal performance in general rather than a specific fin geometry, a plate-fin heat sink, one of the most commonly used fin geometries, was designed and manufactured. While there is an outdoor design temperature standard for industrial coolers (ASHRAE, TSE, etc.), since there is no national or international standard for design ambient temperature standards for heat sinks, 30°C and 40°C were selected as the test ambient temperature. Here, it was assumed that these devices are generally around these temperatures. There is no standard for test powers, and many power values were taken into account in the literature, and in this study, they were randomly selected. Table 1 presents the technical specifications of the heat sinks tested, while Fig. 1 provides the technical drawings, photographs, and thermal images of the heat sinks.

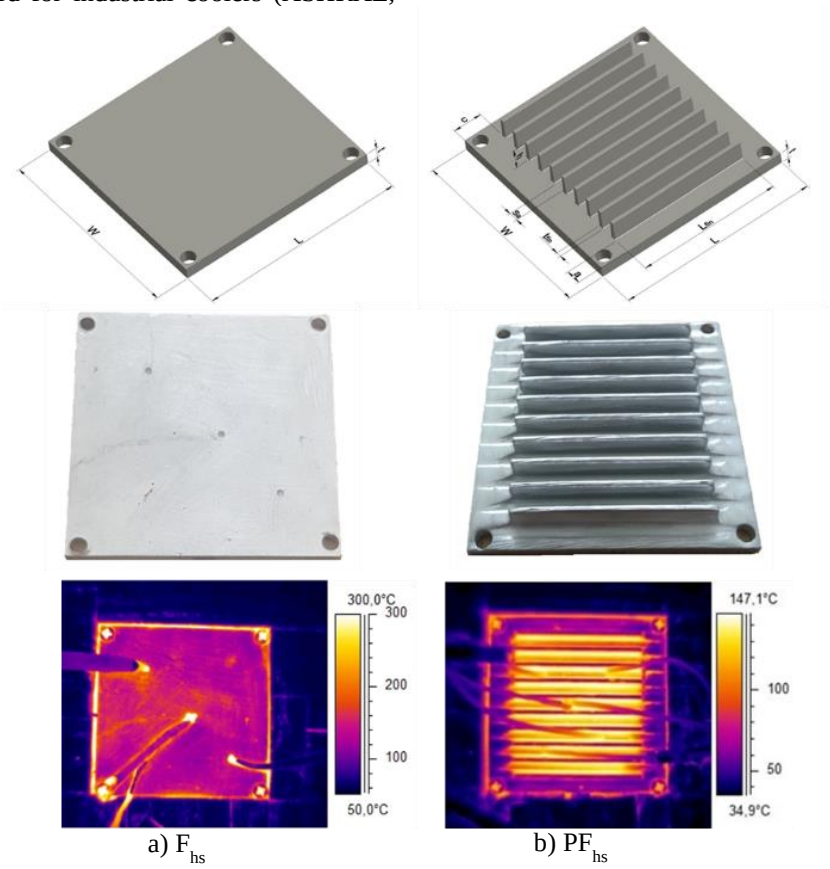

a) F_{hs} b) PF_{hs}

Figure 1. Technical drawing, photograph, and thermal image of F_{hs} and PF_{hs}

Table 1. Technical specifications of HSs.

Heat sink	Base			Fin							Area	Mass
	mm			mm							m^2	G
	W	L	t	no	h	L_{fin}	t_{fin}	s_a	a	c		
PF_{hs}	80	80	5	10	10	54	2.6	4.33	7.5	13	0.0177	114.3
F_{hs}	80	80	5	-	-	-	-	-	-	-	0.0064	83.8

The thermal performance tests of the heat sinks under natural convection conditions were conducted at ambient temperatures of 30°C and 40°C, with heating powers of 16.5 W and 33 W. The experimental setup for natural convection is shown in Fig. 2, which includes a photograph and a schematic diagram. The experimental setup consists of an ambient heater with a thermostat, a test platform, heating resistance, a power supply, a thermal camera, a data logger, and temperature sensors. During the tests, two thermostat-controlled electric heaters were used to maintain a constant ambient temperature. The experiment commenced once the

ambient temperature reached the predefined temperature. The ambient temperature was measured using two thermocouples and PT1000-type temperature sensors. A custom-made heating resistance (80x80x3 mm) was controlled by an adjustable DC power supply to deliver the specified heat loads to the heat sinks. A 150x150x30 mm firebrick was prepared with a slot at its geometric center to accommodate the heat sink and heating resistance, with the test models placed accordingly. The bottom and sides of the heat sink slot were insulated with felt insulation (k:0.0336 W/mK), and the surrounding area was further insulated with polyurethane foam. Three thermocouples were placed in a channel on the bottom surface of the heat sink to measure the junction temperature. For surface temperature measurements, three thermocouples were used for the flat model, while six were used for the finned model—three on the base plate and three on the fins. A thermal camera was positioned 200 mm away from the heat sinks for measurements. The technical specifications of the measurement devices used in the thermal performance tests of the heat sinks are provided in Table 2.

Table 2. Technical specifications of heat sink models.

Sensor/Device	Model	Range/specification	Accuracy
Thermocouple	Elimko	-35+250 °C, T-type	±0.5 °C
Temperature sensor	Comet SN234	-50+200 °C, PT1000 type	±0.15 °C
Thermal camera	FLIR SC325	-20-350 °C	±2 °C or ±2%
Thermostat		220V, 50Hz, 10A, -50+110 °C	±0.03 °C
Multimeter	CHY 21	Digital Multimeter	±(0.5%+1 digit) V ±(1.0%+1 digit) A
Heater	BYM Resistance	DC 0-24 V, max 190 W	
DC power supply	Sayntech 23003	0-30 V x 2 and 5 V, 0-5 A x 2 and 3 A	
Universal data logger	Comet MS6D	16 inputs	
Scales	Extent JCS-B	Maks. 3 kg	0.1 g

During the experiment, the ambient heater was first turned on to allow the environment to reach the specified temperature of 30°C, which took approximately one hour. Once the target temperature was achieved, the measurement devices in the experimental setup and the heating resistance of the heat sink were activated. The setup was operated at the initial test power of 16.5 W for 4 hours, followed by an increase to 33 W, where it was operated for an additional 4 hours. This procedure was repeated separately for an ambient temperature of 40°C. The system took about 3 hours to reach a steady state and was maintained in this regime for approximately 1 hour. The experimental setup and its schematic diagram are shown in Fig. 2.

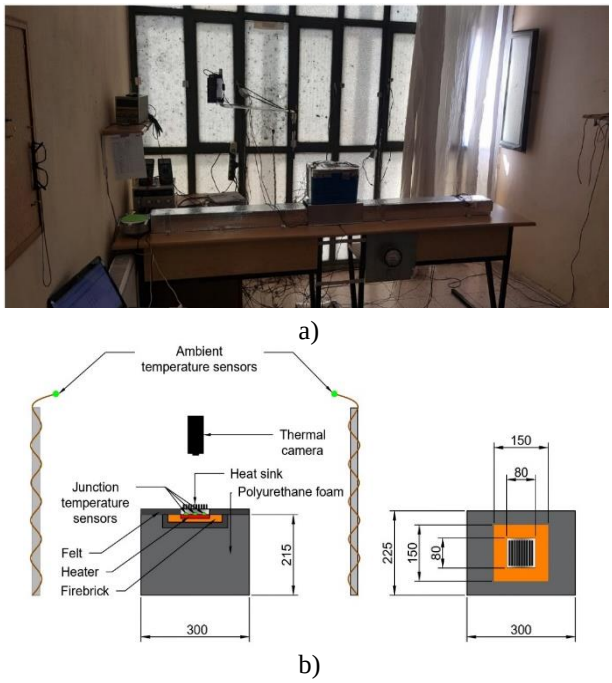

Figure 2. (a) Experimental setup, (b) Schematic view.

2.2. Thermal analyses

The thermal power applied to the heat sink, denoted as $\dot{Q}_{in}$, is equal to the electrical power of the heating resistor, $\dot{Q}_{EP}$. The electrical power can be expressed using the current (I) and voltage (V) values as follows:

$$\dot{Q}_{EP} = \dot{Q}_{in} = IV \quad (1)$$

The heat transfer from the surface of the heat sink to the surrounding environment occurs through convection and radiation. Heat loss due to conduction from the edges and base of the heat sink to the environment is neglected. Therefore, the heat transfer from the heat sink to the surroundings can be expressed as follows:

$$\dot{Q}_{in} = \dot{Q}_{con} + \dot{Q}_{rad} \quad (2)$$

Here, $\dot{Q}_{con}$ represents the convective heat transfer, and $\dot{Q}_{rad}$ represents the heat transfer through radiation, which can be expressed as:

$$\dot{Q}_{rad} = \frac{\sigma A_{hs}({T_{surf}}^4 - {T_{surw}}^4)\varepsilon_s}{(1-\varepsilon_s)+\frac{A_{hs}}{A_{surw}}} \quad (3)$$

In this equation, σ is the Stefan-Boltzmann constant, and A_{hs} is the total heat transfer surface area where both radiation and convection occur. A_{surw} represents the area of the surrounding air wall, T_{surf} is the average surface temperature, T_{surw} is the temperature of the surrounding environment, and ε_s is the emissivity of the surface. The convective heat transfer rate can be calculated as follows:

$$\dot{Q}_{con} = hA_{hs}\eta_o(T_{bp} - T_a) \quad (4)$$

In this equation, h denotes the average convective heat transfer coefficient, T_{bp} is the base plate temperature, T_a is the ambient temperature, and η_o represents the overall fin efficiency, which is calculated as:

$$\eta_o = 1 - \frac{A_{fin}}{A_{hs}}(1 - \eta_f) \quad (5)$$

The fin efficiency η_f is given by:

$$\eta_f = \frac{T_{fin}-T_a}{T_{bp}-T_a} \quad (6)$$

The Nusselt number Nu is defined as:

$$Nu = {hL}/{k} \quad (7)$$

where L is the characteristic length and k is the thermal conductivity of the air. The Rayleigh number Ra is the ratio of buoyancy-driven convection to viscous resistance and is calculated as:

$$Ra = \frac{g\beta(T_{surf}-T_a)L^3}{\nu\alpha} \quad (8)$$

Here, g is the acceleration due to gravity, β is the thermal expansion coefficient of the air, ν is the kinematic viscosity, and α is the thermal diffusivity of the air. The thermophysical properties of the air are considered at the film temperature, T_{film}, calculated as:

$$T_{film} = \frac{T_a+T_{surf}}{2} \quad (9)$$

The average surface temperature of the heat sink, T_{surf}, is calculated as:

$$T_{surf} = \frac{A_{bp}T_{bp}+A_{fin}T_{fin}}{A_{hs}} \quad (10)$$

where A_{bp} is the area of the base plate without fins, A_{fin} is the total fin area, and T_{fin} is the average fin temperature.

Thermal resistance R_{th}, defined as the ratio of the temperature difference between the heat sink surface and the ambient temperature to the input power, is a key thermal characteristic of the heat sink and can also be expressed as:

$$R_{th} = \frac{T_{surf}-T_a}{\dot{Q}_{in}} \quad (11)$$

The total heat transfer coefficient h_T is related to the thermal resistance and is calculated as follows:

$$\frac{1}{h_T A_{hs}} = R_{th} = \frac{T_{surf}-T_a}{\dot{Q}_{in}} \quad (12)$$

The total heat transfer coefficient h_T is expressed as:

$$h_T = \frac{1}{R_{th}A_{hs}} \quad (13)$$

The uncertainties in the experimentally determined thermal resistance, convective heat transfer coefficient, and overall fin efficiency are calculated using the following equation:

$$W_R = \left[\left(\frac{\partial R}{\partial x_1}w_1\right)^2 + \left(\frac{\partial R}{\partial x_2}w_2\right)^2 + \cdots + \left(\frac{\partial R}{\partial x_n}w_n\right)^2\right]^{1/2} \quad (14)$$

Based on the calculations, the maximum uncertainties for thermal resistance, convective heat transfer coefficient, and overall fin efficiency are 2.37%, 1.84%, and 1.05%, respectively.

3. Results and Discussion

This section presents the heat transfer characteristics of the heat sink under natural convection conditions. The experiments were conducted at ambient temperatures of 30°C and 40°C with heating powers of 16.5 W and 33 W. The time-dependent average surface temperature (T_{surf})

Celal Bayar University Journal of Science
Volume 20, Issue 3, 2024, p 91-99
Doi: 10.18466/cbayarfbe.1532575

and junction temperature (T_j) for the specified ambient temperature and heating power under natural convection are shown in Fig. 3. The experimental measurement data generally exhibited stable behavior. The temperature curves reached a steady state after approximately 180 minutes. Naturally, the highest temperature curve corresponds to the junction temperature, with the average surface temperature following a similar trend at a lower level.

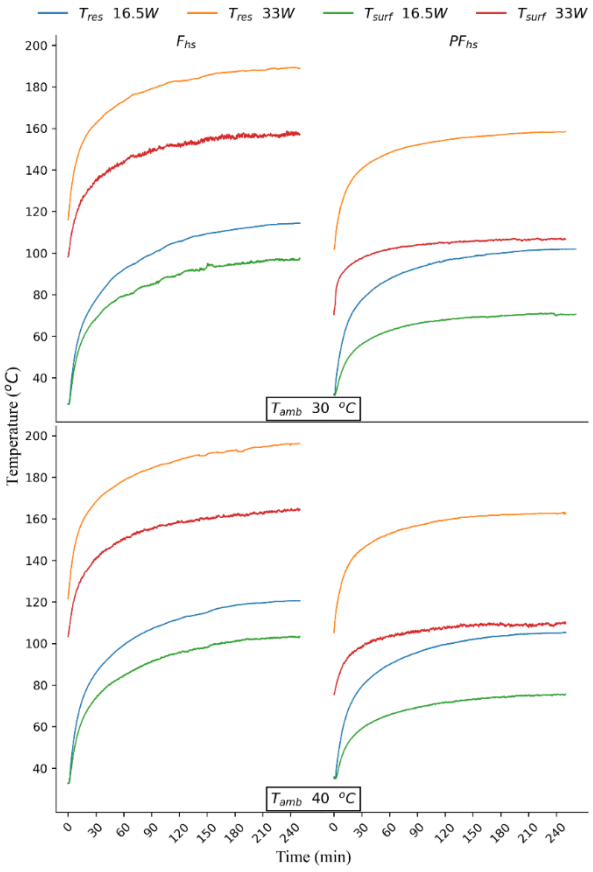

Figure 3. Time-dependent temperature measurement data.

To better understand the situation, Fig. 4 and Fig. 5 present the junction and surface temperatures data based on the average values during the steady-state period (last 60 minutes). For the same heating powers, both junction and surface temperatures increased with the rise in ambient temperature. In the 16.5 W experiment, the junction temperature in the F_{hs} increased from 115.68°C to 120.68°C as the ambient temperature rose from 30°C to 40°C, while at 33 W, it increased from 189.97°C to 196.65°C. In other words, the ambient temperature rise at the same power level also raised the junction temperature, which for the F_{hs} was 5°C at 16.5 W and 6.68°C at 33 W. For the PF_{hs}, the junction temperature increased from 101.6°C to 105.15°C in the 16.5 W experiment and from 157.75°C to 162.22°C at 33 W as the ambient temperature increased. This difference was 3.55°C at 16.5 W and 4.47°C at 33 W.

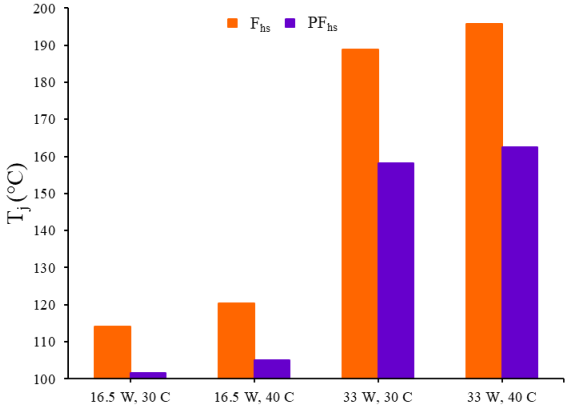

Figure 4. Variation of junction temperature depending on ambient temperature and thermal power.

For the surface temperature, in the case of the PF_{hs}, the temperature increased from 70.67°C to 75.43°C with an ambient temperature rise from 30°C to 40°C at 16.5W power, and from 106.87°C to 109.09°C at 33W power. The temperature rise difference for the PF_{hs} was 4.76°C at 16.5W and 2.22°C at 33W. For the F_{hs}, considering the surface temperature, the temperatures increased from 97.91°C to 103.26°C with an ambient temperature rise at 16.5W, and from 158.78°C to 164.69°C at 33W. The temperature rise difference for the F_{hs} was 5.35°C at 16.5W and 5.91°C at 33W. When considering the ambient temperature increase for the same heating powers, both the junction and surface temperatures of the PF_{hs} increased, but this increase was not as significant as in the F_{hs}. This indicates that the larger surface area of PF_{hs} positively affects the heat transfer performance, resulting in less increase in junction and surface temperatures with rising ambient temperatures compared to the flat type. Specifically, at 16.5W, the temperature difference between the two types with ambient temperatures of 30°C and 40°C is approximately 27°C, while at 33W, the temperature difference between them ranges from 45°C to 55°C.

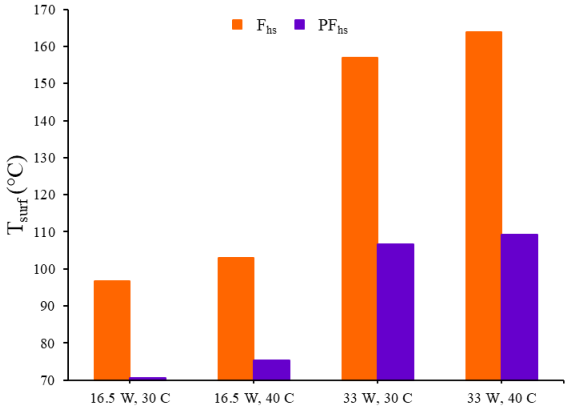

Figure 5. Variation of surface temperature depending on ambient temperature and thermal power.

Fig. 6 shows the results of thermal resistance. Generally, the thermal resistance decreases slightly with increasing ambient temperature and thermal power. The thermal resistance of the F_{hs} typically hovers around 4 K/W, whereas for the PF_{hs}, it ranges between 2-2.5 K/W. For the F_{hs}, the thermal resistance decreases from 4.09 K/W to 3.93 K/W with an increase in ambient temperature from 30°C to 40°C at 16.5W and from 3.88 K/W to 3.83 K/W at 33W. For the PF_{hs}, the thermal resistance decreases from 2.38 K/W to 2.24 K/W with an increase in ambient temperature from 30°C to 40°C at 16.5W and from 2.31 K/W to 2.15 K/W at 33W. This indicates that the 10°C increase in ambient temperature results in an approximate 2-6°C increase in the heat sink surface temperatures.

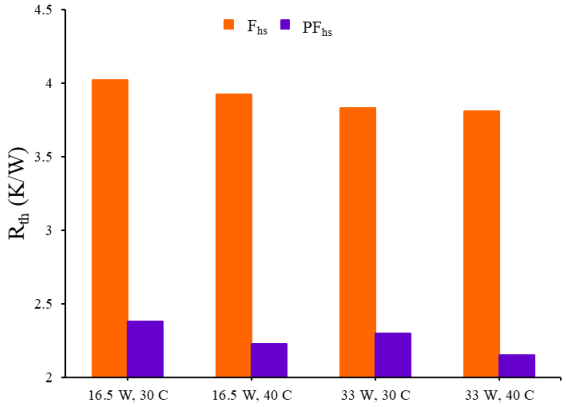

Figure 6. Variation of thermal resistance depending on ambient temperature and thermal power.

Fig. 7 presents the convective heat transfer coefficients. A slight increase in convective heat transfer coefficient values was observed for the same power levels with rising ambient temperature. The coefficients for the F_{hs} are around 30 W/m²K, whereas for the PF_{hs}, the coefficients are around 22 W/m²K. More specifically, for the F_{hs}, the coefficients increase from 28.97 W/m²K to 30.10 W/m²K with an ambient temperature rise from 30°C to 40°C at 16.5W, and slightly increase from 30.14 W/m²K to 30.47 W/m²K at 33W. For the PF_{hs}, the convective heat transfer coefficient rises from 21.44 W/m²K to 22.74 W/m²K with an ambient temperature increase from 30°C to 40°C at 16.5W and slightly increases from 21.87 W/m²K to 23.59 W/m²K at 33W. The coefficient increase difference for the F_{hs} with an ambient temperature rise from 30°C to 40°C is 1.13 and 0.33 W/m²K for the respective power levels. For PF_{hs}, the coefficient increase difference with an ambient temperature rise from 30°C to 40°C is 1.30 and 1.72 W/m²K for the respective power levels.

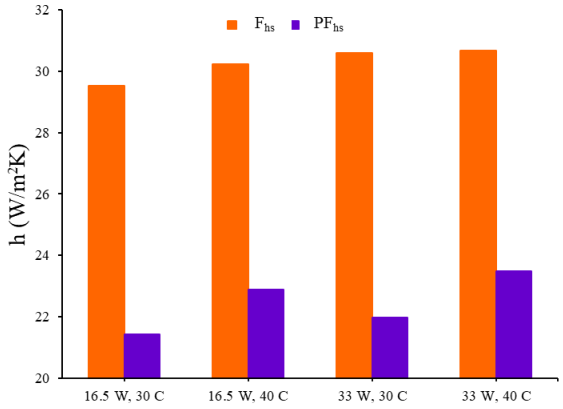

Figure 7. Variation of Convective heat transfer coefficient depending on ambient temperature and thermal power.

Fig. 8 shows the variation of the Nusselt number with thermal power and ambient temperature. The Nusselt number for the F_{hs} hovers around 20.5, while the PF_{hs} hovers around 16. For the F_{hs}, the Nusselt number slightly increases from 20.42 to 20.86 with an ambient temperature rise from 30°C to 40°C at 16.5W, while it slightly decreases from 19.72 to 19.62 at 33W. For the PF_{hs}, the Nusselt number increases slightly from 15.63 to 16.33 with an ambient temperature rise from 30°C to 40°C at 16.5W and from 15.23 to 16.23 at 33W.

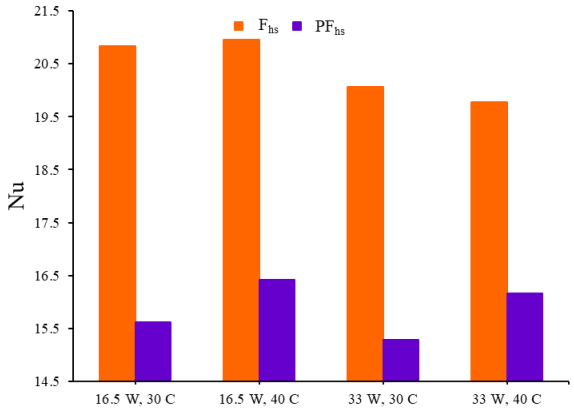

Figure 8. Variation of Nusselt number depending on ambient temperature and thermal power.

Table 3 summarizes the data calculated based on the experimental results. The Prandtl number, defined as the ratio of momentum diffusivity to thermal diffusivity or, in other words, the ratio of the thickness of the velocity boundary layer to the thermal boundary layer, is 0.72 for all experimental conditions with the PF_{hs}. For the F_{hs}, it is also 0.72 in the 16.5 W experiments, similar to the plate model, while it slightly decreases to 0.71 in the 33 W experiments.

The Grashof number, defined as the ratio of buoyancy to viscous forces, is crucial in natural convection studies for

indicating the flow characteristics (laminar or turbulent). Overall, a significant decrease in the Grashof number was observed in all experimental conditions with increasing ambient temperature. More specifically, for the PF_{hs}, the Grashof number decreases from 29076 to 25301 at 16.5 W when the ambient temperature increases from 30°C to 40°C and from 44497 to 38810 at 33 W. For the F_{hs}, the Grashof number decreases from 41948 to 36966 at 16.5 W and from 54025 to 49150 at 33 W. This suggests that the increase in ambient temperature significantly reduces the Grashof number. The difference in the Grashof number reduction due to the increase in ambient temperature is quite similar for both power levels in the flat model, being around 5000. In the plate model, the effect of ambient temperature increase on the Grashof number is approximately 3800 at 16.5 W, while it is 5700 at 33 W. Therefore, at 16.5 W, a lower Grashof number is observed in the plate model compared to the flat model, while at 33 W, a higher Grashof number is observed.

The Rayleigh number, a dimensionless number indicating the effectiveness of convection under natural conditions, can be described as the ratio of factors that accelerate convection to those that delay it. The Rayleigh number at which convection begins depends on the system's environmental conditions and geometry. According to the experimental results, the Rayleigh number significantly decreases with the rise in ambient temperature under all conditions but increases with the applied thermal power. For the PF_{hs}, the Rayleigh number decreases from 20990 to 18231 at 16.5 W and from 31949 to 27826 at 33 W when the ambient temperature increases from 30°C to 40°C. For the F_{hs}, it decreases from 30160 to 26526 at 16.5 W and from 38510 to 34975 at 33 W. The difference in the Rayleigh number reduction due to ambient temperature in the F_{hs} is 3634 at 16.5 W, slightly decreasing to 3535 at 33 W. The same applies to the PF_{hs}, where the reduction difference is 2759 at 16.5 W and 4123 at 33 W. This shows that the decrease in Rayleigh number becomes more pronounced and more affected in the plate model with increasing power.

One of the thermal characteristics of the heat sink, the fin efficiency, was slightly negatively impacted in the plate-fin model when the ambient temperature increased from 30°C to 40°C, dropping from 0.63 to 0.62 at 16.5 W and from 0.65 to 0.64 at 33 W. A very slight increase is observed when considering the effect of increased thermal power on fin efficiency.

Table 3. Calculated dimensionless parameters.

	Ambient temperature	**30 °C**		**40 °C**	
	Heat input	16.5 W	33 W	16.5 W	33 W
PF_{hs}	Prandtl	0.72	0.72	0.72	0.72
	Grashof	29099	44326	25188	38907
	Rayleigh	21007	31826	18150	27894
	η_o	0.76	0.77	0.75	0.77
	η_f	0.63	0.65	0.62	0.64
F_{hs}	Prandtl	0.72	0.71	0.72	0.71
	Grashof	41484	53856	36912	49095
	Rayleigh	29831	38399	26488	34939

4. Conclusion

The thermal performance of the PF_{hs}, compared to the F_{hs}, was experimentally tested under natural convection conditions at thermal power levels of 16.5 W and 33 W and ambient temperatures of 30°C and 40°C. The main findings from this study are summarized below:

- The heat sink's ability to transfer heat to the environment depends on the ambient temperature, which ideally represents the minimum temperature the heat sink can reach. When analyzing fin efficiency and overall fin efficiency at different power levels and ambient temperatures, the values appear close to each other. This result suggests that as the ambient temperature increases, the surface and junction temperatures will also rise.
- For the same heating powers, the surface and junction temperatures increased as the ambient temperature rose from 30°C to 40°C, but the increase was not as significant as the rise in ambient temperature. The increase in junction temperature for the F_{hs} was 5°C at 16.5 W and 6.68°C at 33 W. For the PF_{hs}, the increase in junction temperature was 3.55°C at 16.5 W and 4.47°C at 33 W. The increase in surface temperature for the F_{hs} was 5.35°C at 16.5 W and 5.91°C at 33 W, while for the PF_{hs}, it was 4.76°C at 16.5 W and 2.22°C at 33 W. From this, it can be concluded that the larger surface area of the PF_{hs} positively influenced heat transfer performance, resulting in less increase in junction

and surface temperatures compared to the flat type, and making it less affected by the ambient temperature rise. This was also a key factor in the noticeable difference in junction and surface temperature levels between the flat and PF_{hs}s.

- Regarding thermal resistance, a slight decrease was observed with increasing ambient temperature, parallel with the thermal power. The thermal resistance for the F_{hs} hovered around 4 K/W, whereas it ranged between 2-2.5 K/W for the PF_{hs}. Thus, the PF_{hs} provided an approximately two-fold advantage in thermal resistance compared to the flat type.
- The Nusselt number values for the F_{hs} were around 20.5, while for the PF_{hs}, they were around 16. This can be attributed to the fact that the heat transfer area of the flat type is noticeably smaller compared to the plate model.
- The Rayleigh number significantly decreased with increasing ambient temperature under all conditions but increased with the applied thermal power. This indicates that the increase in the Rayleigh number due to the increase in power was more pronounced in the plate model, showing that it was more affected.
- The fin efficiency in the plate-fin model was slightly negatively affected by the ambient temperature increase, decreasing from 0.63 to 0.62 at 16.5 W and 0.65 to 0.64 at 33 W.

Based on the perspective gained from this experimental study, future research could focus on the effects of fin height, fin spacing, and modifications on the fins.

Acknowledgement

The authors declare that they have no known competing financial interests or personal relationships that could have appeared to influence the work reported in this paper.

Author's Contributions

Mesut Abuşka: Conceptualization, Formal analysis, Investigation, Methodology, Project administration, Resources, Software, Visualization, Writing - original draft, Writing - review & editing.
Vahit Çorumlu: Conceptualization, Formal analysis, Investigation, Methodology, Resources, Software, Visualization, Writing - original draft, Writing - review & editing.

Ethics

There are no ethical issues after the publication of this manuscript.

References

[1]. Khattak, Z., Ali, H. M. 2019. Air cooled heat sink geometries subjected to forced flow: A critical review. *International Journal of Heat and Mass Transfer*, 130: 141-161.

[2]. Doğan, M., Doğan, D. 2017. Experimental investigation of natural convection heat transfer from fin arrays for different tip-to-base fin spacing ratios. *Isı Bilimi ve Tekniği Dergisi*, 37(1): 147-157.

[3]. Haghighi, S. S., Goshayeshi, H. R., Safaei, M. R. 2018. Natural convection heat transfer enhancement in new designs of plate-fin based heat sinks. *International Journal of Heat and Mass Transfer*, 125: 640-647.

[4]. Shen, Q., Sun, D., Xu, Y., Jin, T., Zhao, X. 2014. Orientation effects on natural convection heat dissipation of rectangular fin heat sinks mounted on LEDs. *International Journal of heat and mass transfer*, 75: 462-469.

[5]. Şevik, S., Özdilli, Ö. Study of the effect of fin geometry on the performance of a plate-fin heat sink, In 2nd International African Conference on Current Studies of Science, Technology Social Sciences, Abuja, Nigeria, 2020 pp 315-328.

[6]. Özdilli, Ö., Şevik, S. 2021. Effect of channel and fin geometries on a trapeze plate-fin heat sink performance. *Proceedings of the Institution of Mechanical Engineers, Part E: Journal of Process Mechanical Engineering*, 235(5): 1326-1336.

[7]. Yalçın, B. 2015. Soğutucu Plakalarda Yüzey Geometrisinin ve Kanatçık Sayısının Isı İletimine Etkisinin Sonlu Eleman Analizi İle Araştırılması. *Uluslararası Teknolojik Bilimler Dergisi*, 7(3): 27-39.

[8]. Feng, S., Shi, M., Yan, H., Sun, S., Li, F., Lu, T. J. 2018. Natural convection in a cross-fin heat sink. *Applied Thermal Engineering*, 132: 30-37.

[9]. Banerjee, B., Chattrejee, S., Das, S., Datta, J. 2022. Steady State Free Convection through some Variable Fin Geometries. *YMER* 21(7): 952-959.

[10]. Altun, A. H., Ziylan, O. (2019). Experimental investigation of the effects of horizontally oriented vertical sinusoidal wavy fins on heat transfer performance in case of natural convection. *International Journal of Heat and Mass Transfer*, 139: 425-431.

[11]. Charles, R., Wang, C. C. (2014). A novel heat dissipation fin design applicable for natural convection augmentation. *International Communications in Heat and Mass Transfer*, 59: 24-29.

[12]. Do, K. H., Kim, T. H., Han, Y. S., Choi, B. I., Kim, M. B. (2012). General correlation of a natural convective heat sink with plate-fins for high concentrating photovoltaic module cooling. *Solar Energy*, 86(9): 2725-2734.

[13]. Çorumlu, V. (2024). The effects of input power and ambient temperature on the thermal performance of conical pin fin heat sink in natural convection. *International Journal of Thermal Sciences*, 197, 108855.